Journal of Thermal Analysis and Calorimetry
https://doi.org/10.1007/s10973-020-09339-x

Crystal structure and thermal decomposition kinetics of 1,3,5-trinitro-4,6-diazidobenzene

Peilan Wang[1] · **Jingqi Wang**[2] · **Jianlong Wang**[1]

Received: 7 August 2019 / Accepted: 13 January 2020

Abstract

Two different single crystals of 1,3,5-trinitro-4,6-diazidobenzene ($C_6HN_9O_6$) were measured by X-ray single-crystal diffraction. The molecular weight of $C_6HN_9O_6$ is 295.16. Crystal *I* system is orthorhombic, and space groups are Pbca, $a = 10.5199$ (19) nm, $b = 13.436$ (3) nm, $c = 15.235$ (3) nm, $\beta = 90°$, $V = 2153.4$ (7) nm^3, $Z = 8$, Dc = 1.821 g cm^{-3}, $\mu = 0.164$ mm^{-1}, $F(000) = 1184$. Crystal *II* system is tetragonal, and space groups are P42/no $a = b = 19.412$ (5) nm, $c = 5.9603$ (17) nm, $\beta = 90°$, $V = 2246.0$ (13) nm^3, $Z = 8$, Dc = 1.746 g cm^{-3}, $\mu = 0.157$ mm^{-1}, $F(000) = 1184$. Enthalpy of formation and detonation properties were calculated at the DFT-B3LYP/6-311++G ** level. It shows that these two compounds all have good detonation performance, among which crystal I has higher detonation velocity (8.81 km s^{-1}) and detonation pressure (34.65 GPa) than those of crystal II. *The thermal behavior of the* crystal I was studied by differential scanning calorimetry (DSC)–thermal gravimetric (TG) analysis, melting peak is at 94.80 °C, and two decomposition exothermic peaks are at 126.39 °C and 212.10 °C, respectively, in DSC curve. According to the Kissinger and Flynn–Wall–Ozawa methods, the activation energy (*E*) calculated for the first decomposition of the *crystal I* is 109.25 kJ mol^{-1} and 110.67 kJ mol^{-1}, respectively, and second decomposition is 121.05 kJ mol^{-1} and 124.35 kJ mol^{-1}, respectively. In addition, the accelerating rate calorimeter (ARC) was used to further study the adiabatic decomposition behavior. The *E* of the two decompositions is 128.70 kJ mol^{-1} and 302.55 kJ mol^{-1}, respectively, and the pre-exponential (*A*) is 1.02×10^{16} s^{-1} and 2.01×10^{35} s^{-1}, respectively, by ARC data. The mechanism functions were $f(\alpha) = 2\alpha^{0.5}$ (first decomposition) and $f(\alpha) = 3\alpha^{2/3}$ (second decomposition).

Keywords 1,3,5-trinitro-4,6-diazidobenzene · Crystal structure · Detonation parameters · Thermal decomposition kinetics

Introduction

Compared with traditional explosives, such as TNT, RDX, and HMX, nitrogen-rich compounds have excellent performance including high nitrogen content, high enthalpy of formation, safety, and environmentally friendly. They are applied to high-energy sensitive explosives, rocket propellants, gas-generating composition, and fireworks composition, which broaden the applications of nitrogen-rich compounds in energetic material field [1–3]. Azide compounds have a great density and a high burning rate, and per mole of azide group is decomposed to release 314 kJ to 397 kJ [4]. Therefore, it is suitable for using as conventional fuels, jet fuels, and propellant additives. Organic azido is an important active intermediate which can occur click reaction, cycloaddition reaction, and Staudinger ligation [5, 6].

Differential scanning calorimetry (DSC), thermal gravimetric analysis (TG), and accelerating rate calorimeter (ARC) are an effective way to study the thermal decomposition process of a substance. Thermal decomposition kinetic parameters, such as the apparent activation energy and pre-exponential constant, are the main factors for determining the thermal properties of energetic materials. Pourmortazavi et al. [7] studied the thermal stability of NTO and KNF via DSC, and they also studied the effect of nitro on the thermal stability and decomposition kinetics of nitro-HTPB, which revealed that the onset and maximum peak temperatures increased due to the higher nitro content in HTPB and increasing the DSC heating rate leads to the lower thermal stability temperatures of the nitro-HTPB [8]. Pourmortazavi et al. also studied the thermal behavior of energetic materials

✉ Jianlong Wang
wangjianlong@nuc.edu.cn

[1] School of College of Chemical Engineering and Technology, The North University of China, Taiyuan, China

[2] Norinco Group Hubei DongFang Chemical Industry Co. Ltd, Xiangyang, China

when nanometer metal oxide is used as propellant [9, 10]. Li et al. researched the thermal properties of 3,5-dinitro-1-oxygen-3,5-diazacyclohexane by DSC–TG technology. The result shows that the 3,5-dinitro-1-oxygen-3,5-diazacyclohexane is a low melting point compound with excellent stability [11]. Zhang et al. [12] discussed the thermal properties of TNT and DNAN by ARC, which indicating that DNAN has a relatively better thermal stability than TNT.

1,3,5-Trinitro-4,6-diazidobenzene (DATNB) is a high-energy nitrogen-rich organic compound and an important intermediate. 1,3,5-trinitro-4,6-diazidobenzene was originally made by British with 1,3,5-trinitro-4,6-dichlorobenzene (DCTNB) and sodium azido in methanol and acetone mixed system, the yield was 95%, and the melting point was 92–94 °C after refining [13]. Huo and Lv obtained DATNB by reacting of DCTNB and sodium azide in dimethyl sulfoxide. The yield of DATNB was 90.9% [14, 15].

In this paper, the 1,3,5-trinitro-4,6-diazidobenzene (DATNB) was synthesized from DCTNB. Its structure was characterized by elemental analysis, Fourier-transform infrared (FT-IR) spectroscopy, nuclear magnetic resonance (NMR) spectroscopy, and mass spectrometry (MS) [16]. The structure is further confirmed by X-ray single-crystal diffraction. The detonation parameters of DATNB are an important criterion for evaluating the performances of an energetic material. Hence, we calculate the detonation velocity based on the theoretical density of different crystal forms. To the best of our information, there is no report about the thermal decomposition kinetics of DATNB. This is the study of the detonation parameters, thermal decomposition kinetics, and decomposition mechanism functions of DATNB.

Experimental

General information

All regents used in experiments such as acetone, methanol, dimethyl sulfoxide, ethyl acetate, and petroleum ether were analytically pure and purchased from Institute of Chemical Reagents in Tianjin and used without further purification. Deionized water was self-made in the laboratory. The elemental analysis was carried out on PE instrument (Model CHNO-2000). 1H-NMR spectra were recorded on a 300 MHz Bruker instrument with Acetone-*d*6 solvents. The FT-IR spectra were measured on a VERTEX 80 produced by Bruker in Germany. MS spectra were carried on a Q Exactive Mass Spectrometer produced by Thermo Fisher Scientific Company in Germany. Single-crystal X-ray diffraction data were collected on an Agilent Xcalibur & Gemini made by Agilent in America. Thermal analysis was carried out on a METTLER DSC 3 and NETZSCH TG 209F1 Libra and ES-Accelerating Rate Calorimeter.

Preparation of DATNB crystals

1,3,5-Trinitro-4,6-diazidobenzene samples were synthesized as proposed previously by Ref. 13. Changing the ratio of material and solvent, 2.82 g (0.01 mol) of 1,3,5-trinitro-4,6-dichlorobenzene was placed in a 100-mL four-necked flask, 25.40 mL of acetone and methanol was separately added, and a solution of sodium azide (1.50 g) in water (5.4 mL) and methanol (5.4 mL) was added dropwise. The reaction was carried out at room temperature for 1 h. Then, the solution was poured into ice water, and a solid was collected, washed, and dried. The yield was 98.6%. The melting point is 92–94 °C. Anal. FT-IR spectrum of DATNB is observed in Fig. 1. FT-IR (KBr): 1552.92, 1338.92 (C–NO_2), 3088.88 (Ar–H), 2160.77 (N≡N). Calcd. (%) for $C_6HN_9O_6$: C, 24.41; H, 0.34; N, 42.71; O, 32.54. Found (%): C, 24.50; H, 0.36; N, 43.28; O, 31.86. 1H NMR (Acetone-*d*6) δ: 8.937 (s, 1H Ar–H). ^{13}C NMR (151 MHz, Acetone-*d*6) δ: 137.80, 133.38, 125.51, 125.22. EI-MS: *m*/*z* 296 (M−).

The azide group is easily affected by light. The produced pale yellow solid turns red under the light [17]. The red solid was dissolved in ethanol, and the bulk crystal I is obtained by solvent evaporation at room temperature. The needle crystal II was obtained by dissolving the pale yellow solid in ethanol and evaporating with solvent at room temperature.

Crystal data and structure determination

Two crystals with different crystal forms were obtained at room temperature by solvent evaporation. Crystal I (0.22 mm × 0.15 mm × 0.08 mm) was a bulk crystal, and crystal II (0.19 mm × 0.08 mm × 0.03 mm) was needle. The two crystals were selected to determine their structure by Bruker SMART APEX CCD 6000 area detector diffractometer equipped with a graphite monochromator Mo $K\backslash\alpha$ radiation ($\lambda = 0.71073$ Å). The two temperatures are 173 K and 150 K, respectively. For I, a total of 1,2965 diffraction spots were collected in the range of $2.674° \leq \theta \leq 26.409°$ by *w*-scan scanning, of which 1740 [$I > 2\sigma(I)$] were observable diffraction spots, and 2198 [$R_{\text{int}} = 0.0191$] diffraction points were for structure analysis and refinement. For II, in the range of $1.484° \leq \theta \leq 24.995°$, a total of 1,5461 diffraction points were collected by *f* and *w* scans, including 1981 [$I > 2\sigma(I)$] observed ones and 1107 [$R_{\text{int}} = 0.0191$] diffraction points were for structural analysis and refinement. All parameters were corrected by L_P factors and empirical absorption. The crystal structure was analyzed using the SHELXL-97 program [18] and optimized using the SHELXL-97 program [19]. The details of data collection and refinement are given in Table 1.

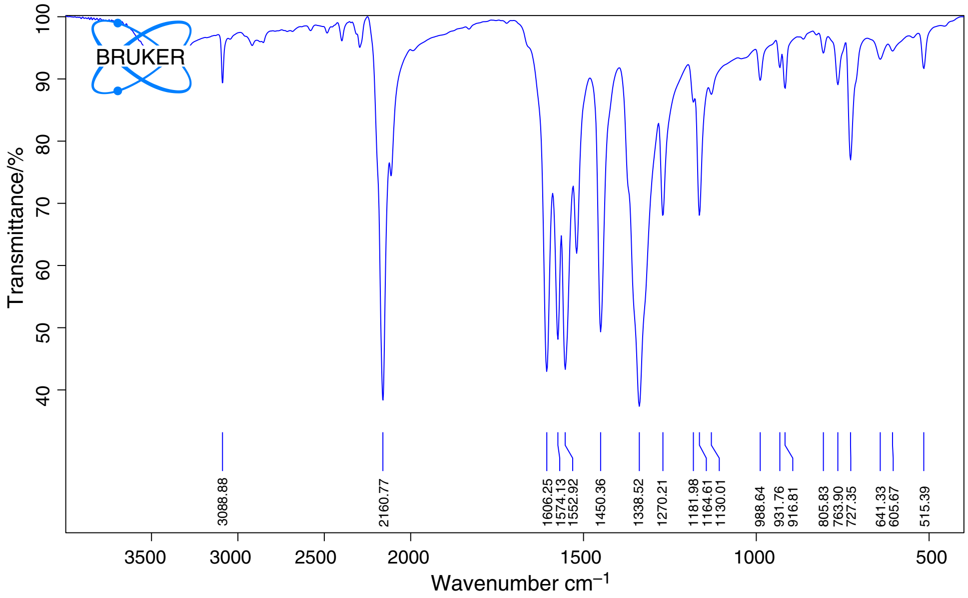

Fig. 1 FT-IR spectrum of the prepared DATNB

Table 1 Crystal data and structure refinement for DATNB

Item	Value	
	Crystal I	Crystal II
Empirical formula	$C_6HN_9O_6$	$C_6HN_9O_6$
Formula mass	295.16	295.16
Temperature/K	173	150
Crystal system	Orthorhombic	Tetragonal
Crystal size/mm^3	0.22 × 0.15 × 0.08	0.19 × 0.08 × 0.03
Space group	Pbca	P42/n
a/nm	10.5199 (19)	19.412 (5)
b/nm	13.436 (3)	19.412 (5)
c/nm	15.235 (3)	5.9603 (17)
β/°	90	90
V/nm^3, Z	2153.4 (7), 8	2246.0 (13), 8
Dc/g cm^{-3}	1.821	1.746
M/mm^{-1}	0.164	0.157
F(000)	1184	1184
θ/°	2.674–26.409	1.484–24.995
h, k, and l range	− 13–13, − 16–16, − 16–19	− 22–23, − 23–23, − 7–7
Independent reflection (R_{int})	0.0191	0.0191
Goodness of fit on F^2	1.047	1.056
R, wR ($I > 2\sigma(I)$)	0.0435, 0.1243	0.0756, 0.1763
R, wR (all data)	0.0564, 0.1355	0.1418, 0.2025
($\Delta\rho$)max, ($\Delta\rho$)min/e nm^{-3}	0.317, − 0.260	0.264, − 0.345

Calculation of detonation velocity and pressure

The detonation parameters, density, and heat generation of energetic compounds can predict the detonation performance and safety of energetic compounds. Detonation velocity and pressure are an important indicator of the performance of energetic materials. The density directly determines the detonation velocities and pressures. The two different crystal forms of DATNB have different theoretical densities. The detonation performance can be reflected by detonation velocity and pressure. Enthalpy of formation and detonation properties were calculated at the DFT-B3LYP/6-311++G** level. The detonation velocities and detonation pressures were predicted by the Kamlet formula [20].

Thermal experimental instruments and conditions

Thermal analysis was performed using a DSC, TG, and ARC instruments. DSC experiments are carried out with mg-scale samples, and the heat evolved or consumed in the reaction is estimated under isothermal conditions Therefore, the thermal data obtained from DSC can be used as a baseline data in determining safe operating temperatures because of the non-adiabatic experimental conditions. The sample of crystal I (~ 1 mg) was placed in a crucible and heated from 25 to 400 °C at the heating rates of 5, 10, 15, and 20 °C min^{-1} in a nitrogen atmosphere. Crystal I has the same thermal decomposition behavior as crystal II, and there is no crystal transformation.

ARC is a common apparatus to measure the thermal behavior under adiabatic condition. Under adiabatic conditions, the temperature and pressure in the reactor will increase sharply and the samples may explode because the heat generated from material decomposition is all used to heat up the material itself. Therefore, it can supply more safety to evaluate the materials under adiabatic condition [21]. The specific heat capacity was estimated by the law of science as 1.50 J g^{-1} °C^{-1} [22]. The sample of crystal I (0.198 g) was placed in a titanium alloy ball and heated from 50 to 300 °C, the heating rate was 1.1 °C min^{-1}, the heating step was 5 °C, the waiting time was 15 min, and the temperature rise rate sensitivity was 0.02 °C min^{-1}.

Results and discussion

Crystal structure description

The analysis of single crystal shows that this 1,3,5-trinitro-4,6-diazidobenzene belongs to orthorhombic and tetragonal crystal system with space group Pbca or P42/*n* with *Z*=8. Due to the different crystal systems, the density of crystal I is 1.821 g cm^{-3}, and the crystal II is 1.746 g cm^{-3}. The molecular structures and packings are shown in Fig. 2–4. Three parameters including bond lengths, bond angles, and torsion angles are shown in Tables 2 and 3.

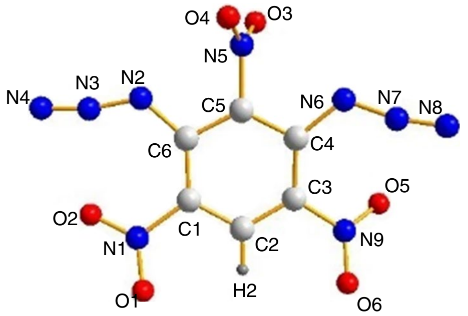

Fig. 2 Molecular structure of the DATNB

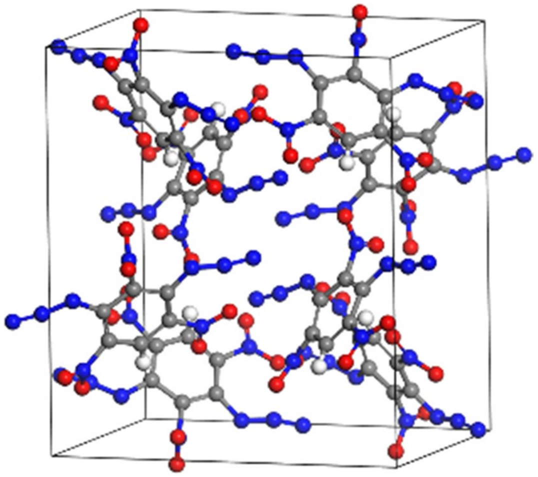

Fig. 3 Molecular packing in crystal I

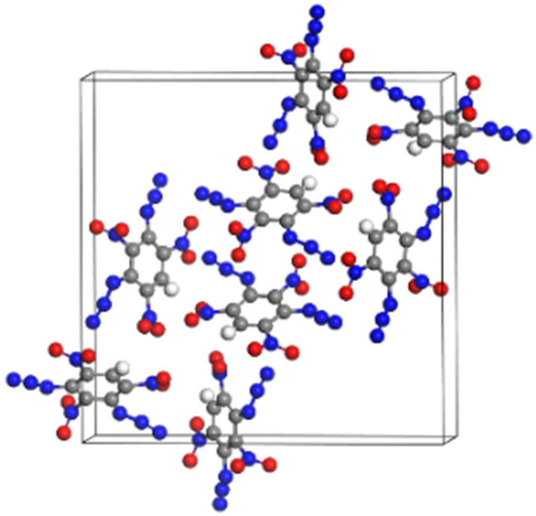

Fig. 4 Molecular packing in crystal II

As shown in Fig. 2, the two azide groups and the three nitro groups are connected to C6, C4, C1, C3, and C5, respectively. Figures 3 and 4 show that there are eight ordered molecular structures of DATNB in a unit cell. The bond lengths of N9–C3 and N2–C6 are 1.4644 (24)° and 1.3800 (25)°, respectively (listed in Table 2), which are shorter than the average bond length of C–NO_2 (1.468Å). However, it found that the C5–N5 is 1.4730 (27) Å, which is longer than 1.468Å, indicating that the nitro groups on C3 and C6 are more stable [23]. In addition, in Table 2, the bond angles indicate that the structure of DATNB is symmetry. Table 3 shows that the torsion angles of C1–C2–C3–C4, C2–C3–C4–C4, C3–C4–C5–C6, and C4–C5–C6–C1 of crystal I are 4.566 (276)°, – 7.017 (261)°, 3.713 (268)°, and – 6.406 (249)°, respectively, and those of the crystal II are – 5.895 (700)°, 3.539 (600)°, 0.532 (623)°, and 0.088

Table 2 Bond lengths and bond angles of DATNB

Crystal I				Crystal II			
Bond	Dist./Å	Bond	Dist./Å	Bond	Dist./Å	Bond	Dist./Å
O1–N1	1.2080 (23)	C5–N5	1.4730 (27)	O1–N1	1.2071 (69)	C5–N5	1.4756 (56)
O2–N1	1.2136 (23)	N7–N8	1.1129 (25)	O2–N1	1.2258 (68)	N7–N8	1.1212 (69)
C1–N1	1.4579 (23)	N7–N6	1.2598 (24)	C1–N1	1.4368 (61)	N7–N6	1.2562 (55)
N3–N4	1.1088 (31)	N6–C4	1.3889 (25)	N3–N4	1.1096 (71)	N6–C4	1.3817 (58)
N2–N3	1.2266 (26)	O5–N9	1.2236 (24)	N2–N3	1.2321 (60)	O5–N9	1.2121 (60)
N2–C6	1.3800 (25)	O6–N9	1.2176 (23)	N2–C6	1.3765 (55)	O6–N9	1.2257 (66)
O4–N5	1.2020 (29)	N9–C3	1.4644 (24)	O4–N5	1.2091 (54)	N9–C3	1.4788 (55)
O3–N5	1.2064 (28)	C2–C3	1.3726 (25)	O3–N5	1.2094 (52)	C2–C3	1.3642 (65)
C2–C1	1.3833 (25)	C1–C6	1.4099 (25)	C2–C1	1.3816 (70)	C1–C6	1.4112 (56)
C6–C5	1.4032 (25)	C5–C4	1.3941 (26)	C6–C5	1.3783 (57)	C5–C4	1.4008 (55)
C4–C3	1.4023 (26)	C2–H2	0.9501 (18)	C4–C3	1.3970 (58)	C2–H2	0.9506 (51)
Angle	°	Angle	°	Angle	°	Angle	°
C1–C6–C5	114.876 (159)	C3–C4–C5	115.805 (169)	C1–C6–C5	114.777 (366)	C3–C4–C5	114.995 (352)
C2–C1–C6	120.958 (162)	C2–C3–C4	120.770 (166)	C2–C1–C6	119.839 (386)	C2–C3–C4	120.155 (403)
N1–C1–C2	115.349 (147)	N9–C3–C2	116.522 (157)	N1–C1–C2	227.366 (401)	N9–C3–C2	117.740 (402)
N1–C1–C6	123.662 (155)	N9–C3–C4	122.363 (163)	N1–C1–C6	122.661 (374)	N9–C3–C4	121.998 (352)
N2–C6–C1	133.837 (170)	N6–C4–C3	130.775 (173)	N2–C6–C1	132.346 (372)	N6–C4–C3	131.43 (39)
N2–C6–C5	111.287 (155)	N6–C4–C5	113.415 (156)	N2–C6–C5	112.83 (358)	N6–C4–C5	113.572 (359)

Table 3 Torsion angles of DATNB

Crystal I				Crystal II			
Torsion angle	°	Torsion angle	°	Torsion angle	°	Torsion angle	°
O1–N1–C1–C2	13.840 (241)	N3–N4–C6–C1	−4.856 (361)	O1–N1–C1–C2	−26.200 (673)	N3–N4–C6–C1	−18.501 (762)
O4–N5–C5–C6	75.057 (254)	N7–N6–C4–C3	−13.959 (322)	O4–N5–C5–C4	−81.798 (485)	N7–N6–C4–C3	21.667 (703)
O5–N9–C3–C4	−27.544 (260)	C1–C2–C3–C4	4.566 (276)	O5–N9–C3–C2	24.614 (609)	C1–C2–C3–C4	−5.895 (700)
C2–C3–C4–C5	−7.017 (261)	C3–C4–C5–C6	3.713 (268)	C2–C3–C4–C5	3.539 (600)	C3–C4–C5–C6	0.532 (623)
C4–C5–C6–C1	−6.406 (249)			C4–C5–C6–C1	0.088 (582)		

(582)°, respectively. The data show that the coplanarity of the six atoms of the benzene ring is strong. Furthermore, the torsion angles of O1–N1–C1–C2, N3–N4–C6–C1, O4–N5–C5–C6, N7–N6–C4–C3, and O5–N9–C3–C4 of crystal I are 13.840 (241)°, −4.856 (361)°, 75.057 (254)°, −13.959 (322)°, and −27.544 (260)°, respectively. For crystal II, the torsion angles of O1–N1–C1–C2, N3–N4–C6–C1, O4–N5–C5–C6, N7–N6–C4–C3, and O5–N9–C3–C4 are −26.200 (673)°, −18.501 (762)°, −81.798 (485)°, 21.667 (703)°, and 24.614 (609)°, respectively. The data indicate that the five groups are not in the same plane with the benzene ring. However, compared with crystal I, dihedral angles of crystal II between the groups attached to C1, C4, C5, C6 of the benzene ring are larger. Due to the influence of space steric, the dihedral angle of nitro group has changed. In addition, there is a strong *π*–*π* stacking in the molecule, and the intramolecular and intermolecular hydrogen bonds are weak.

Table 4 Properties of DATNB, RDX, and HMX

Compound	M/g mol^{-1}	ρ/g cm^{-3}	Q/kcal g^{-1}	D/km s^{-1}	P/GPa
Crystal I (DATNB)	292	1.821	1.80	8.81	34.65
Crystal II (DATNB)	292	1.746	1.80	8.61	32.49
RDX	222	1.78	1.25	8.86	34.23
HMX	296	1.90	1.25	9.10	34.40

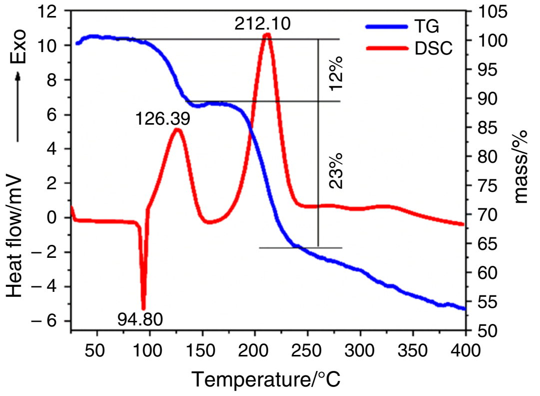

Fig. 5 DSC–TG curves of DATNB

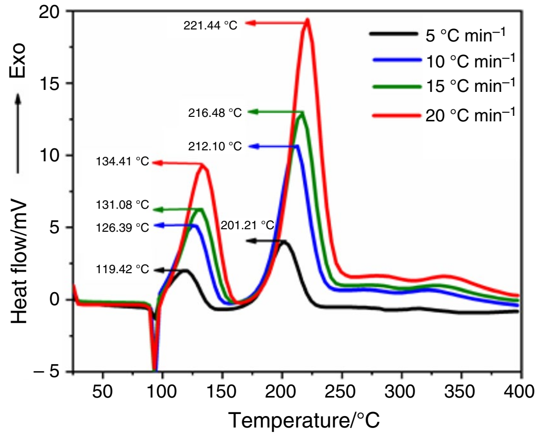

Fig. 6 Effect of DSC heating rate on decomposition temperature of investigated energetic samples

Calculation results of detonation parameters

For comparison, detonation parameters of DATNB, RDX, and HMX are calculated simultaneously. The results are shown in Table 4.

Table 4 shows that the detonation velocity and pressure of the crystal I (DATNB) are greater than those of the crystal II (DATNB), which indicates that crystal I has better detonation performance. The detonation heat and detonation pressure of DATNB are greater than RDX and HMX, but the detonation velocity is less than RDX and HMX, indicating that DATNB is an energetic compound with a high detonation heat and a high detonation pressure.

Thus, it can be seen that the azide group can increase the detonation pressure, because azide group can release a large amount of nitrogen gas when the explosion occurs.

Thermal behavior of DATNB

The thermal analysis of DSC–TG results

The typical DSC–TG curves (Fig. 5) indicate that the thermal behaviors of title compound can be described in three stages which contain an endothermic and two exothermic processes.

It shows that the melting endothermic peak of the compound is 94.80 °C, followed by two exothermic decomposition peaks at 126.39 °C and 212.10 °C, respectively. In the TG curve, there are two stages of mass loss, of which the first mass loss is 12% and the second mass loss is 23%, which is consistent with the two exothermic stages on the DSC curve. In addition, the decomposition starts after melting, and the ΔH_d of the two processes are 899.38 J g^{-1} and

Table 5 First decomposition kinetics basic data of DSC

β/K min^{-1}	T_P/K	$10^3 T_P^{-1}$/K^{-1}	Kissinger method In (β/T_P^2)/min^{-1} K^{-1}	FWO method lg β/K min^{-1}
5	392.57	2.55	− 10.34	0.70
10	399.54	2.50	− 9.68	1.00
15	404.17	2.47	− 9.30	1.18
20	407.56	2.45	− 9.02	1.31

Table 6 Second decomposition kinetics basic data of DSC

β/K min^{-1}	T_P/K	$10^3 T_P^{-1}$/K^{-1}	Kissinger method In (β/T_P^2)/min^{-1} K^{-1}	FWO method lg β/K min^{-1}
5	474.36	2.11	− 10.71	0.70
10	485.25	2.06	− 10.07	1.00
15	489.63	2.04	− 9.68	1.18
20	494.59	2.02	− 9.41	1.31

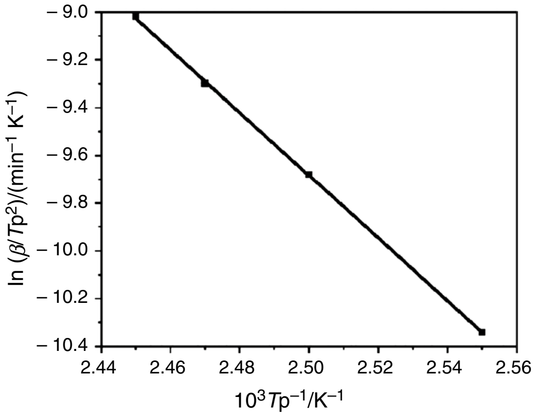

Fig. 7 $\ln(\beta/T_P^2)$ versus T_P^{-1} by Kissinger method for first decomposition

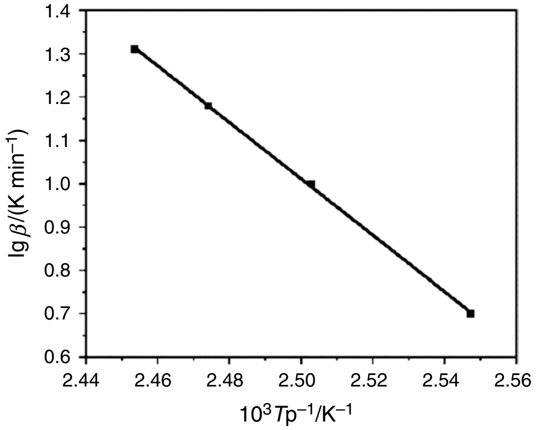

Fig. 8 $\ln\beta$ versus T_P^{-1} by FWO method for first decomposition

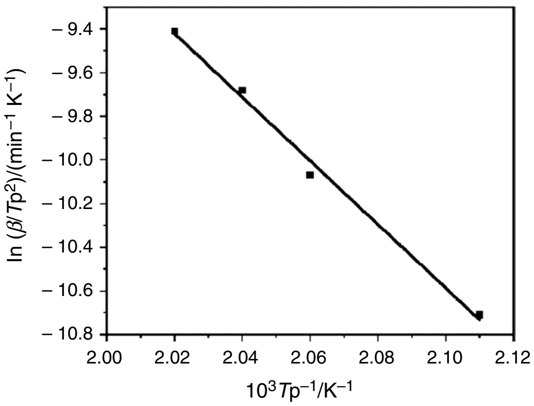

Fig. 9 $\ln(\beta/T_P^2)$ versus T_P^{-1} by Kissinger method for second decomposition

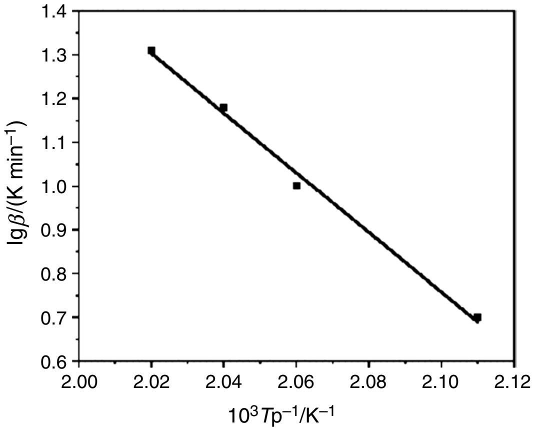

Fig. 10 $\ln\beta$ versus T_P^{-1} by FWO method for second decomposition

1835.25 J g^{-1}, respectively. Figure 4 shows that the onset temperature of the second decomposition is very close to the end temperature of the first decomposition. So, we can conclude that of the title compound is easy to lead to fierce secondary decomposition during the decomposition process.

Figure 6 presents DSC curves for decomposition of the studied energetic samples at different heating rates. As seen in this figure, decomposition peaks of the samples were shifted to the higher temperatures by increasing the heating rate. The data of β and T_P at two decomposition stages are shown in Tables 5 and 6.

Kissinger and Flynn–Wall–Ozawa methods which are two integral methods [24–26] are used to calculate the kinetic parameters (the apparent activation energy (E) and pre-exponential constant (A)) of the title compound.

Kissinger Eq. (1) and Flynn–Wall–Ozawa Eq. (2) are described as follows:

$$\ln\left(\frac{\beta}{T_P^2}\right) = \ln\left(\frac{AR}{E}\right) - \frac{E}{RT_P} \tag{1}$$

$$\log\beta = \log\left[\frac{AE}{RG(\alpha)}\right] - 2.315 - \frac{0.4567E}{RT_P} \tag{2}$$

where β is the linear heating rate (K min^{-1}), T_P is the peak temperature of the DSC curves (K), A is the pre-exponential constant (s^{-1}), R is the gas constant (J mol^{-1} K^{-1}), E is the apparent activation energy (kJ mol^{-1}), and $G(\alpha)$ is the integral form of reaction mechanism function.

Figures 7 and 8 are fitted from the data in Table 5. Figure 7 shows a fitting curve correlated by Kissinger equation, which illustrates the relationship between $\ln(\beta/T_P^2)$ and T_P^{-1}. The slope and intercept of the line are − 13.14 and 23.16,

Table 7 Kinetics parameters of title compound

	E_k/kJ mol^{-1}	A/s^{-1}	r_k^2	E_o/kJ mol^{-1}	r_o^2
First decomposition	109.25	2.50×10^{15}	0.9998	110.67	0.9998
second decomposition	121.05	2.38×10^{12}	0.9937	124.35	0.9940

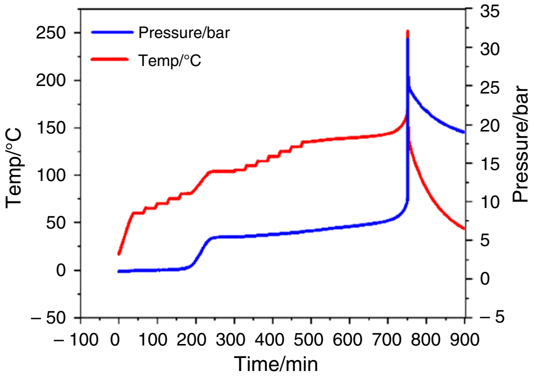

Fig. 11 Temperature and pressure versus time

respectively, and the correlation coefficient (r^2) is 0.9998. Therefore, the first decomposition activation energy E_{k1} and pre-exponential constant A calculated by the Kissinger method are 109.25 kJ mol^{-1} and 8.33×10^{16} s^{-1}, respectively. Using Flynn–Wall–Ozawa method, the relationship between lgβ and T_P^{-1} is graphically illustrated in Fig. 8. The slope and intercept of the line we obtained from the Flynn–Wall–Ozawa equation are −6.07 and 16.19, respectively, with a correlation coefficient of 0.9998. So, activation energy E_{o1} of the first decomposition obtained by the Flynn–Wall–Ozawa method is 110.67 kJ mol^{-1}.

Figures 9 and 10 are fitted from the data in Table 6. The slope and intercept of the line in Fig. 9 are − 14.56 and 20.00, respectively, and the correlation coefficient is 0.9937. Thus, E_{k2} and A of the second-order decomposition acquired using the Kissinger method are 121.05 kJ mol^{-1} and 2.38×10^{12} s^{-1}. In Fig. 10, −6.82 and 15.08 are the slope and intercept of the Flynn–Wall–Ozawa method, respectively, with a correlation coefficient (r^2) of 0.9940. Finally, the E_{o2} of second decomposition stage is 124.35 kJ mol^{-1}.

The kinetic parameters values (E and A) determined by the Kissinger and the Flynn–Wall–Ozawa method are shown in Table 7. We can see that the E obtained by Kissinger method agrees well with these obtained by the Flynn–Wall–Ozawa method, and the correlation coefficient (r^2) is close to 1, indicating the satisfactory validity of the results. The lower apparent activation (Table 7) of title compound indicates that less energy is required in its thermal decomposition, so it exists unstably. Therefore, the temperature of synthesis and storage of the compound are worthy of attention.

The thermal analysis of ARC results

The adiabatic decomposition parameters of title compound have been studied by ARC. Figures 11 and 12 show the results of the test.

As shown in Figs. 11 and 12, after five H–W–S periods, the first self-decomposition reaction of DATNB starts at 80.6 °C. (The temperature rise rate is 0.08 °C min^{-1}.) The temperature rise rate reaches a maximum of 1.05 °C min^{-1} after 49.5 min, and the temperature and pressure are 101.31 °C and 4.83 bar, respectively. After that, the self-heating rate decreases due to the consumption of reactants. The first stage of heat release ends at 103.91 °C. The second exotherm starts at 135.67 °C (the temperature rise rate is 0.08 °C min^{-1}) after several H–W–S modes. The temperature rise rate is 4158.6 °C min^{-1} when the temperature is 214.88 °C, after 232.43 min. The pressure rise rate is not detected because it is too large. The reason may be that DATNB decomposes rapidly and produces

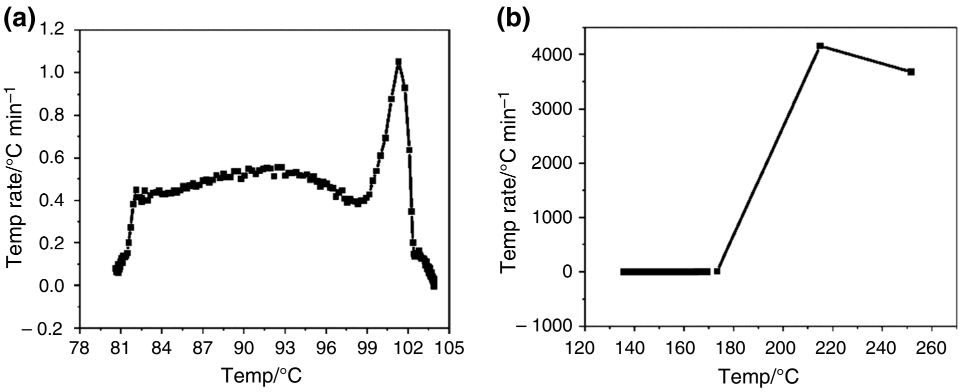

Fig. 12 Decomposition temperature rate verse temperature; **a** first decomposition **b** second decomposition

Table 8 Self-heating decomposition parameters of DATNB by ARC

Parameters	First stage		Second stage	
	Values	Corr.	Values	Corr.
Onset temperature/°C	80.60	–	135.67	–
Onset temperature rate/°C min^{-1}	0.08	0.97	0.03	0.36
Max self-heating rate/°C min^{-1}	1.05	12.62	4158.62	49,986.61
Temperature at max rate/°C	101.31	–	214.88	–
Final temperature/°C	103.91	360.79	251.66	1650.19
Adiabatic temperature rise/°C	23.31	280.19	126.00	1514.52
Time to maximum rate/min	49.50	4.12	232.43	19.34
Onset pressure/bar	1.52	–	6.21	–
Pressure at max rate/bar	4.83		10.54	–

large amounts of gas products. It should be note that the high temperature rise rate and pressure rise rate indicate that the released energy may be generated and then explode if the decomposition of DATNB occurs uncontrolled in a confined space.

During the exothermal decomposition, the measuring vessel is also hated up. This means that the self-heating rate is decreased by the measuring vessel compared to measurement without measuring vessel. Therefore, it is necessary to correct the tested parameters. The corrected and measured self-heating decomposition parameters of DATNB are given in Table 8. The formulas of the inertia factor ϕ and the corrected characteristic parameters are defined as follows [27, 28]:

$$\varnothing = 1 + \frac{M_b \times C_{vb}}{M_S \times C_{vs}} \tag{3}$$

$$\Delta T_s = \varnothing \Delta T \tag{4}$$

$$m_{0s} = \varnothing m_0 \tag{5}$$

$$T_{fs} = T_0 + \varnothing \Delta T \tag{6}$$

$$\theta_s = \frac{\theta}{\varnothing}. \tag{7}$$

where M_b is the mass of the bomb, C_{vb} is the specific heat of bomb, M_s is the mass of the sample, and C_{vs} is the specific heat of reaction sample. ΔT is the adiabatic temperature rise, m_0 is the initial self-heating rate, T_0 is the initial decomposition temperature, θ is the time to maximum rate, and subscript s is the corrected value.

Table 8 shows that the thermal decomposition temperature of DATNB is lower and the released energy is higher. The time of the start of thermal decomposition and the maximum thermal decomposition rate is 4.12 and 19.34 min, respectively. It is proved that there is no strong autocatalytic phenomenon in its thermal decomposition.

In addition, in real situations, energetic materials may suffer the adiabatic decomposition: ammunition with big size and low heat conductivity, energetic materials heated up by forced heating and showing a temperature increase in their center by heat accumulation (as in slow cook-off). In comparison with DSC, ARC can determine the self-heating of samples in an adiabatic environment. In this way, the decomposition process is controlled by sample rather than forced from an outside temperature program, which is similar to the real adiabatic decomposition. ARC determines the self-heating decomposition of the sample in an adiabatic environment with large sample amounts. Therefore, the ARC measurements were implemented to research the adiabatic thermal decomposition mechanism functions of DATNB. Activation energy (E) and pre-exponential factor (A) of the sample are calculated under adiabatic conditions by rate constant method and mechanism functions method. For an nth-order reaction with a single reaction, the self-heat rate (SHR) of adiabatic system can be expressed as follows [29]:

$$k^* = kC_0^{n-1} = \frac{m_T}{\left[\frac{T_f - T}{\Delta T_{ad}}\right]^n \Delta T_{ad}} \tag{8}$$

where k^* is the pseudozero-order rate constant at the temperature T, C_0 is the initial concentration of the reactant, T is the temperature at time t, m_T is the temperature rate at the temperature T, ΔT is the adiabatic temperature rise, and n is the reaction order.

Arrhenius equation:

$$k^* = Ae^{\frac{-E}{RT}} \tag{9}$$

where A is the apparent pre-exponential factor, and E is apparent activation energy.

By substituting and rearranging Eq. (9) into Eq. (8), We can get the following:

$$\ln k^* = \ln \frac{m_T}{\left[\frac{T_f - T}{\Delta T}\right]^n \Delta T} = \ln A - \frac{E}{RT} \tag{10}$$

According to Eq. (10), the curves of Ink^* versus T^{-1} for the self-heating decomposition of DATNB are illustrated in

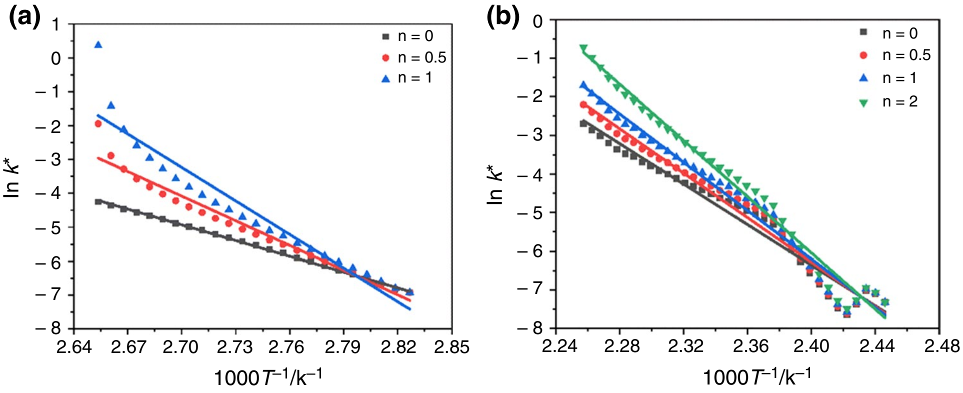

Fig. 13 ln k^* versus T^{-1} of DATNB **a** first decomposition; **b** second decomposition

Table 9 Adiabatic kinetics parameters of first decomposition of DATNB

n	E_a/kJ mol^{-1}	A/s^{-1}	r^2
0	128.70	1.02×10^{16}	0.9987
0.5	201.53	4.49×10^{26}	0.9612
1	274.45	2.00×10^{37}	0.9147

Table 10 Adiabatic kinetics parameters of second decomposition of DATNB

n	E_a/kJ mol^{-1}	A/s^{-1}	r^2
0	218.16	3.89×10^{24}	0.9632
0.5	239.28	1.84×10^{27}	0.9707
1	260.39	8.80×10^{29}	0.9762
2	302.55	2.01×10^{35}	0.9832

Table 11 16 types of thermal decomposition mechanism functions

Item	$f(\alpha)$
1	$1/(2\alpha)$
2	$2\alpha^{0.5}$
3	$1-\alpha$
4	$(1-\alpha)^2$
5	$2(1-\alpha)^{3/2}$
6	$[-\mathrm{In}(1-\alpha)]^{-1}$
7	$1.5(1-\alpha)^{2/3}[1-(1-\alpha)^{1/3}]^{-1}$
8	$1.5(1+\alpha)^{2/3}[(1+\alpha)^{1/3}-1]^{-1}$
9	$1.5(1-\alpha)[-\mathrm{In}(1-\alpha)]^{1/3}$
10	$4(1-\alpha)[-\mathrm{In}(1-\alpha)]^{3/4}$
11	$3\alpha^{2/3}$
12	$3(1-\alpha)^{2/3}$
13	$2(1-\alpha)^{1/2}$
14	$3(1-\alpha)[-\mathrm{In}(1-\alpha)]^{2/3}$
15	$2(1-\alpha)[1-\mathrm{In}(1-\alpha)]^{1/2}$
16	$(2/3)[(1-\alpha)^{-1/3}-1]^{-1}$

Fig. 13. The activation energy and the pre-exponential factor are calculated from the linear relationship of ln k^*–T^{-1}, and they are listed in Tables 9 and 10.

The apparent activation energy and pre-exponential factor of adiabatic decomposition process are also calculated by using mechanism functions method that comes from Achar–Brindley–Sharp method. After taking logarithm, formula 11 is deformed as follows:

$$\ln\left[\frac{m_{\mathrm{T}}}{f(\alpha)}\right] = \ln(A\Delta T_{\mathrm{ad}}) - \frac{E}{RT} \tag{11}$$

where T is the temperature; $m_{\mathrm{T}} = \mathrm{d}T/\mathrm{d}t$ is the temperature rate; ΔT_{ad} is the adiabatic temperature rise; and $f(\alpha)$ symbolizes the kinetic model in the form of differential equation. α symbolizes the reaction degree, $\alpha = (c_0 - c)/c_0 = (T - T_0)/\Delta T_{\mathrm{ad}}$; then, the data are substituted into 16 kinds of thermal decomposition mechanism functions (Table 11), respectively [30, 31]. ln $\left[\frac{m_{\mathrm{T}}}{f(\alpha)}\right]$ versus T^{-1} should give a straight line with a slop $-E/R$ proving the kinetic model which is correctly chosen. The results are shown in Figs. 14 and 15. The liner fitting results are listed in Tables 12 and 13.

Table 12 indicates that, for the first decomposition, the highest correlation coefficient and the corresponding kinetic model are model 2. Table 13 indicates that, for the second decomposition, the highest correlation coefficient and the corresponding kinetic model are model 11.

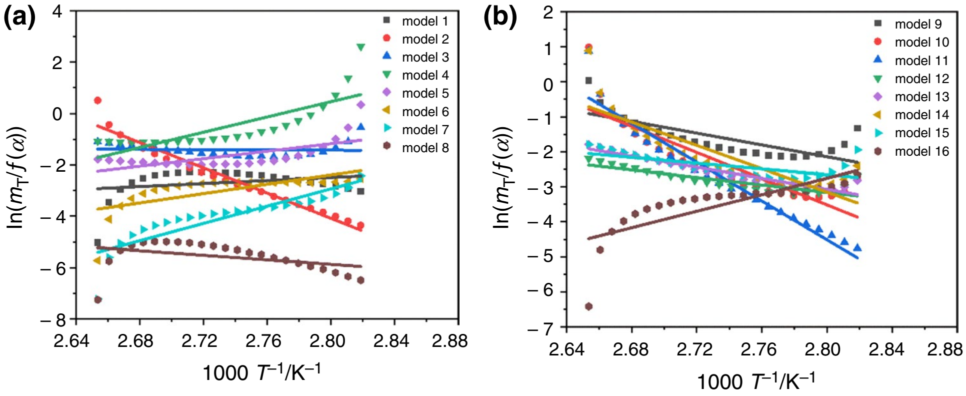

Fig. 14 $\ln((m_T)/(f(\alpha)))$ versus T^{-1} of DATNB first decomposition

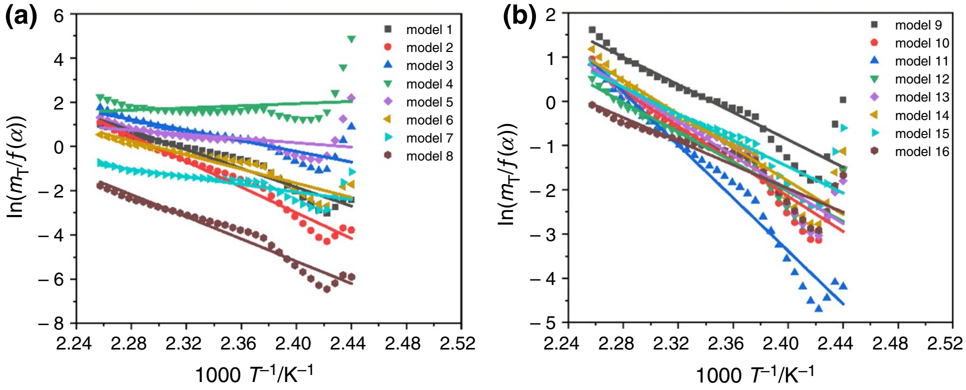

Fig. 15 $\ln((m_T)/(f(\alpha)))$ versus T^{-1} of DATNB second decomposition

Table 12 Kinetic parameter regression results for the first decomposition

Item	r^2	$\ln(A\Delta T_{ad})$	$-E/R$	E/kJ mol^{-1}	A/s^{-1}
1	0.0642	−10.75	2.95	–	–
2	0.9588	64.84	−24.62	204.69	6.19×10^{26}
3	0.0027	−0.66	−0.27	2.24	–
4	0.6397	−41.20	14.88	–	–
5	0.4400	−21.84	7.30	–	–
6	0.4387	−27.84	9.09	–	–
7	0.7660	−0.07	16.83	–	–
8	0.1462	6.45	−4.40	36.58	27.15
9	0.5720	21.51	−8.45	70.25	9.42×10^{7}
10	0.7502	48.74	−18.66	155.14	6.31×10^{19}
11	0.9413	72.99	−27.68	230.13	2.15×10^{30}
12	0.7156	11.75	−5.33	44.31	5.44×10^{3}
13	0.9157	18.91	−7.85	65.26	6.99×10^{6}
14	0.7328	43.38	−16.62	138.18	2.97×10^{17}
15	0.4377	8.87	−4.17	34.67	3.05×10^{2}
16	0.5894	−35.74	11.78	–	–

Table 13 Kinetic parameter regression results for the second decomposition

Item	r^2	$\ln(A\Delta T_{ad})$	$-E/R$	E/kJ mol^{-1}	A/s^{-1}
1	0.9334	49.37	−21.34	177.42	5.07×10^{19}
2	0.9697	66.75	−29.06	241.60	1.79×10^{27}
3	0.7288	28.64	−12.03	100.02	5.04×10^{10}
4	0.0378	−3.90	2.44	–	–
5	0.1975	11.67	−4.80	39.91	2.15×10^{3}
6	0.8972	36.82	−16.04	133.36	1.80×10^{14}
7	0.6438	18.52	−8.58	71.33	2.03×10^{6}
8	0.9532	55.02	−25.09	208.60	1.44×10^{22}
9	0.8283	36.36	−15.51	128.95	1.14×10^{14}
10	0.8970	45.53	−19.87	165.20	1.09×10^{18}
11	0.9719	68.43	−29.92	248.75	9.62×10^{27}
12	0.8837	38.39	−16.85	140.09	8.65×10^{14}
13	0.9204	44.22	−19.26	160.13	2.94×10^{17}
14	0.8863	43.79	−18.99	157.88	1.91×10^{17}
15	0.8223	34.29	−14.90	123.88	1.43×10^{13}
16	0.8464	30.18	−13.40	111.41	2.35×10^{11}

Conclusions

In this study, the synthesis and characterization of the energetic material 1,3,5-trinitro-2,4-diazidobenzene and its crystal structure, detonation parameters, and thermal properties are studied.

1. Crystal I belongs to orthorhombic with the space group of Pbca, $a = 10.5199$ (19) nm, $b = 13.436$ (3) nm, $c = 115.235$ (3) nm, $\beta = 90°$, $V = 2153.4$ (7) nm^3, $Z = 8$, $Dc = 1.821$ g cm^{-3}, $\mu = 0.164$ mm^{-1}, $F(000) = 1184$. Crystal II belongs to tetragonal with the space groups of P42/no. $a = b = 19.412$ (5) nm, $c = 5.9603$ (17) nm, $\beta = 90°$, $V = 2246.0$ (13) nm^3, $Z = 8$, $Dc = 1.746$ g cm^{-3}, $\mu = 0.157$ mm^{-1}, $F(000) = 1184$.
2. The detonation velocity and the detonation pressure of crystal I are 8.81 km s^{-1} and 34.65 GPa, respectively, and those of crystal II are 8.61 km s^{-1} and 32.49 GPa, respectively. The detonation velocity of crystal I is lower than that of RDX and HMX, but the detonation pressure is higher than that of HMX and RDX.
3. The non-isothermal decomposition kinetic and thermodynamic parameters are obtained. The activation energy shows good correction by the Kissinger and Flynn–Wall–Ozawa methods, and the values obtained by Flynn–Wall–Ozawa method are nearly close to those obtained by Kissinger method.
4. The adiabatic decomposition experiment by ARC reveals that the maximum self-heating rate of DATNB is 4158.62 °C min^{-1} at second decomposition. After a long induction period, the reaction will become uncontrollable, which may result in an explosion accident finally. The apparent activated energy calculated under adiabatic condition is 128.70 kJ mol^{-1} ($n = 0$) and 302.55 kJ mol^{-1} ($n = 2$), respectively.
5. Under adiabatic condition, the mechanism functions for decomposition of DATNB are $f(\alpha) = 2\alpha^{0.5}$ (first decomposition) and $f(\alpha) = 3\alpha^{2/3}$ (second decomposition).

Acknowledgements We thank the Center of Testing and Analysis, Shanghai Institute, for support.

References

1. Chavez DE, Hiskey MA, Gilardi RD. 3,3′-Azobis(6-amino-1,2,4,5-tetrazine): a novel high-nitrogen energetic material. Angew Chem Int Ed. 2000;39:1791.
2. Yang SQ, Xu SL, Huang HJ, Zhang W, Zhang XG. High nitrogen compounds and energetic materials. Prog Chem. 2008;20:526–37.
3. Jiang YB, Qi CX, Han CM. Advances in the synthesis of organic azides. Chin J Org Chem. 2016;32:2231–8.
4. Li YC, Zhang XJ, Fu W, Pang SP, Zhang CL. Synthesis, characterization and thermal decomposition of 4,4′,6,6′-tetraazidoazo-1,3,5-triazine (TAAT). Chin J Org Chem. 2012;31:1484–9.
5. Gao FL, Ji YP, Liu WX, Wang YL, Chen B, Liu YJ, Ding F. Synthesis and characterization of pentanol-3-nitraza-5-azidonitrate. Chin J Energy Mater. 2015;23:302–3.
6. Li YC, Zhang XJ, Fu W, Pang SP, Zhao CL. Synthesis, characterization and thermal decomposition mechanism of 4,4′,6,6′-tetra(azido)azo-1,3,5-triazine (TAAT). Chin J Org Chem. 2011;31:1484–9.
7. Pourmortazavi SM, Rahimi-Nasrabadi M, Kohsari I, Hajimirsadeghi SS. Non-isothermal kinetic studies on thermal decomposition of energetic materials. J Therm Anal Calorim. 2012;110(2):857–63.
8. Abusaidi H, Ghaieni HR, Pourmortazavi SM, et al. Effect of nitro content on thermal stability and decomposition kinetics of nitro-HTPB. J Therm Anal Calorim. 2016;124:935–41.
9. Pourmortazavi SM, Mirzajani V, Farhadi K. Thermal behavior and thermokinetic of double-base propellant catalyzed with magnesium oxide nanoparticles. J Therm Anal Calorim. 2018;137:93–104.
10. Mirzajani V, Farhadi K, Pourmortazavi SM. Catalytic effect of lead oxide nano- and microparticles on thermal decomposition kinetics of energetic compositions containing TEGDN/NC/DAG. J Therm Anal Calorim. 2018;131:937–48.
11. Li J, Chen LZ, Wang JL, Lan GC, Hou H, Li M. Crystal structure and thermal decomposition kinetics of byproduct of synthesis of RDX: 3,5-dinitro-1-oxygen-3,5-diazacyclohexane. Acta Phys Chim Sin. 2015;31:2049–56.
12. Zhang CY, Jin SH, Ji JW, Jing BC, Bao F, Zhang GY, Shu QH. Thermal hazard assessment of TNT and DNAN under adiabatic condition by using accelerating rate calorimeter (ARC). J Therm Anal Calorim. 2017;131:89–93.
13. Bailey AS, Case JR. 4:6-dinitrobenzofuroxan, nitrobenzodifuroxan and benzotrifuroxan: a new series of complex-forming reagents for aromatic hydrocarbons. Tetrahedron. 1958;3:113–31.
14. Lu CY, Sheng DL, Chen LK, Huo H, Zhu YH, Yang B. Preparation of ultrafine CL-18 and research on its narrow pulse detonation performance. Chin J Explos Propell. 2013;36:47–50.
15. Huo H, Wang BZ, Zhou C, Zhou YS, Luo YF. Synthesis, characterization and performances of 7-amino-6-nitrobenzodifuroxans. Chin J Org Chem. 2011;31:701–7.
16. Cheng CS, Qin FT, Wei ZY. Chemical safety production and reaction risk assessment. 1st ed. Beijing: Chemical Industry Press; 2011.
17. Budyka FM. Photodissociation of aromatic azides. Russ Chem Rev. 2008;77(8):709–23.
18. Sheldrick GM. SHELXS-97, program for X-ray crystal structure refinement. Göttingen: Göttingen University; 1997.
19. Sheldrick GM. SHELXS-97, program for X-ray crystal structure solution. Göttingen: Göttingen University; 1997.
20. Li YL, Liu TY, Cao DL, Wang JL. Theoretical study on structure and properties of tetranitropyrrole and its derivatives. J Energy Mater. 2017;25:291–7.
21. Tou JC, Whiting LF. The thermokinetic performance of an accelerating rate calorimeter. Thermochim Acta. 1981;48:21–42.
22. Zhao GL, Yan GX. Estimation of thermodynamic data of organic matter. Beijing: Higher Education Publishing Society; 1983. p. 113–4.
23. Allen FH, Kennard O, Watson DG. Tables of bond lengths determined by X-ray and neutron diffraction. Part I. Bond lengths in organic compounds. J Chem Soc Perkin Trans. 1987;7:1–19.
24. Kissinger HE. Reaction kinetics in differential thermal analysis. Anal Chem. 1957;29(11):1702.
25. Ozawa T. A new method of analyzing thermogravimetric data. Bull Chem Soc Jpn. 1965;38(11):1881.

26. Chen LZ, Liu W, Wang JL, Cao DL. Crystal structure and thermal decomposition kinetics of 3-nitro-4-diazo-5-oxygenpyrazole. Chin J Struct Chem. 2018;37:1807–902.
27. Liu W, Liu ZX, Wang JL, Cao DL, Chen LZ. Adiabatic decomposition analysis of 3,4-dinitropyrazole based on accelerating calorimeter. Sci Technol Eng. 2018;18:126–30.
28. Sivapirakasam SP, Nalla Mohamed M, Surianarayanan M, Sridhar VP. Evaluation of thermal hazards and thermo-kinetic parameters of a matchhead composition by DSC and ARC. Thermochim Acta. 2013;557:13–9.
29. Bao F, Zhang GZ, Jin SH. Thermal decomposition behavior and thermal stability of DABT·2DMSO. J Therm Anal Calorim. 2018;131:3185–91.
30. Hu RZ, Gao SL, Zhao FQ, Shi QZ, Zhang TL, Zhang JJ. Kinetics of thermal analysis. 2nd ed. Beijing: Science Press; 2008. p. 79–83.
31. Zhang GY, Jin SH, Li LJ, Li ZH, Shu QH, Wang DQ, Zhang B, Li YK. Evaluation of thermal hazards and thermo-kinetic parameters of 3-amino-4-amidoximinofurazan by ARC and TG. J Therm Anal Calorim. 2016;126:1223–30.